# Effects of Surface Heterogeneity on the Adsorption of $CO_2$ in Microporous Carbons

Yangyang Liu and Jennifer Wilcox*

Department of Energy Resources Engineering, School of Earth Sciences, Stanford University, Green Earth Sciences 065, 367 Panama Street, Stanford, California 94305, United States

**S** *Supporting Information*

**ABSTRACT:** Carbon capture combined with utilization and storage has the potential to serve as a near-term option for $CO_2$ emissions reduction. $CO_2$ capture by carbon-based sorbents and $CO_2$ storage in geologic formations such as coal and shale both require a thorough understanding of the $CO_2$ adsorption properties in microporous carbon-based materials. Complex pore structures for natural organic materials, such as coal and gas shale, in addition to general carbon-based porous materials are modeled as a collection of independent, noninterconnected, functionalized graphitic slit pores with surface heterogeneities. Electronic structure calculations coupled with van der Waals-inclusive corrections have been performed to investigate the electronic properties of functionalized graphitic surfaces. With Bader charge analysis, electronic structure calculations can provide the initial framework comprising both the geometry and corresponding charge information required to carry out statistical modeling. Grand canonical Monte Carlo simulations were carried out to determine the adsorption isotherms for a given adsorbent−adsorbate interaction at temperature/pressure conditions relevant to carbon capture applications to focus on the effect of the surface functionalities. On the basis of the current work, oxygen-containing functional groups were predicted to enhance $CO_2$ adsorption in microporous carbon materials in the absence of water vapor, and the hydrated graphite was found to hinder $CO_2$ adsorption.
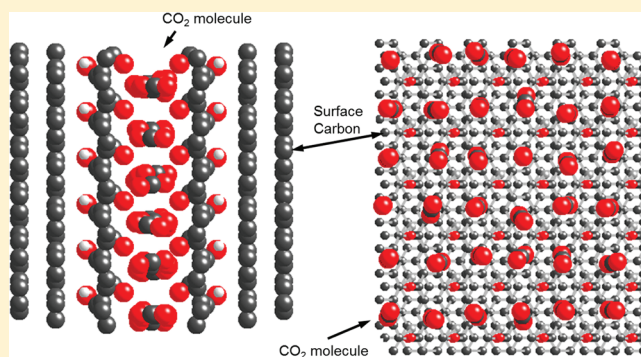
## 1. INTRODUCTION

To mitigate $CO_2$ emissions from coal- and natural-gas-fired power plants, our energy system must ultimately rely on renewable energy sources with minimal carbon emissions.[1] However, technologies based on thermodynamically efficient and economically viable large-scale economic electricity generation from non-carbon-based energy sources are still in development. Therefore, $CO_2$ capture combined with utilization and storage may serve as a bridging strategy to the development of noncarbonized energy systems. $CO_2$ capture by carbon-based sorbents and $CO_2$ storage in geologic formations are two attractive options for $CO_2$ emissions reduction. A number of potential sinks exist for captured $CO_2$,[2] including depleted oil and gas fields, $CO_2$-enhanced oil recovery (EOR), $CO_2$-enhanced gas recovery (EGR), $CO_2$-enhanced coal-bed methane recovery (ECBM), deep saline aquifers, and some other storage options, such as mineral carbonation. It is important to note that enhanced energy resource recovery processes using $CO_2$ do not result in permanent storage of all of the $CO_2$ used. In fact, since $CO_2$ is costly it is economically favorable to recycle as much of the $CO_2$ as possible with each injection process. When $CO_2$ is regulated and capture processes becomes less expensive, there will be incentive to sequester more of the $CO_2$ with these enhanced recovery processes. Both of the capture (by carbon-based sorbents) and storage

processes (in coal and gas shale reservoirs) require a thorough understanding of $CO_2$ adsorption properties in complex micro- and mesoporous carbon-based materials. Although carbon capture and storage are separate processes, at the molecular-scale, they both share a major challenge, i.e., an insufficient fundamental understanding of the processes involving $CO_2$ adsorption in micropores of carbon and the subsequent difficulties in predicting $CO_2$ adsorption capacities. Thus, molecular-level simulations of carbon-based systems with surface functionalities, which can be thought to represent synthetic carbon-based sorbents and organic matter in natural materials with structural and/or chemical heterogeneities, are of interest for both carbon capture and storage applications.

In the case of $CO_2$ storage applications, it is well accepted that coal and the organic components of gas shale are comprised of extremely complex molecular frameworks that vary considerably in pore size, shape, and network. To investigate the process of gas adsorption−desorption using statistical modeling, these complex pore structures of carbon-based porous materials have frequently been modeled as a
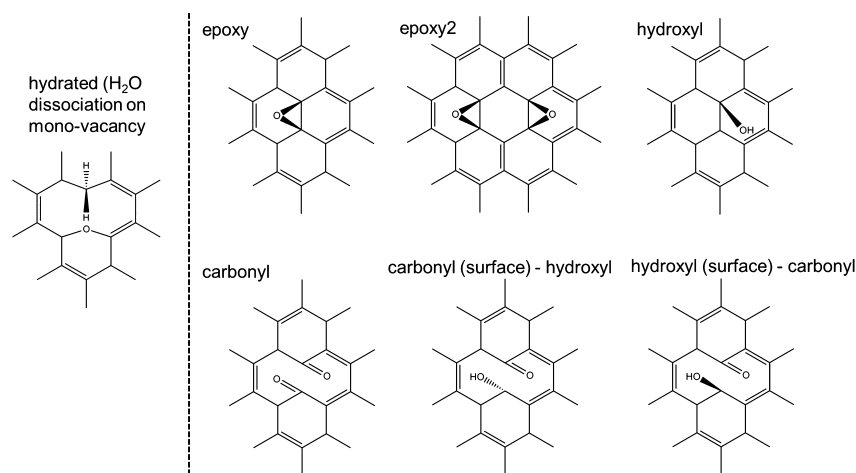
**Figure 1.** Functionalized graphitic surfaces investigated in the current work. These functional groups are positioned in the center of the top layer of the periodic graphite slabs.

collection of independent, noninterconnected slit pores with perfect graphitic walls.[3−10] However, as the disagreement between the modeling and experimental adsorption isotherms suggests, models that do not include structural and chemical heterogeneities fail to accurately predict adsorption capacities.[5,11] Previous experimental studies provide indication that the natural and synthetic carbon-based systems include both aromatic and aliphatic structures, as well as a variety of surface functional groups,[12−14] including volatile components such as water vapor, methane, and nitrogen- and sulfur-containing compounds. Such chemical heterogeneity will likely play an important role in determining the adsorption capacity and adsorbed/gas phase equilibrium properties such as density, heat of adsorption, and packing within the pore. For instance, if the porous carbon materials include a hydroxyl surface functional group at the carbon surface, this could lead to complex $CO_2$– functional group−surface interactions. Rather than interacting directly with a surface, $CO_2$ may react indirectly via a shared proton. Indeed, these embedded functional groups will change the electrostatic properties of the adsorbent surface and thus are expected to play an important role in the adsorption mechanisms associated with $CO_2$ in these systems depending on the temperature and pressure conditions. In the case of carbon capture, the control of surface chemical functionality is essential for the design of effective carbon-based micro- and mesoporous materials. For instance, if the surface functional groups favor $CO_2$ due to the stronger electrostatic interactions, $CO_2$ may be selectively captured from a given gas mixture, e.g., $N_2$, $O_2$, $CH_4$, and $H_2O$. Such investigations will reveal which of these functional groups act to passivate or enhance surface adsorption of $CO_2$. The inclusion of these surface functionalities in the carbon model is required to accurately determine the mechanism of adsorption and subsequent material capacity. Additionally, knowledge of the packing of $CO_2$ in the pore structure and the forces that underlie the existence of the condensed phase will aid in understanding the heats of sorption associated with $CO_2$ in a variety of pores that differ either in size and/or in surface chemistry.

Although the adsorption of $CO_2$ on simplified graphitic surfaces has been experimentally and computationally investigated previously,[15−26] few statistical molecular simulations of $CO_2$ adsorption have taken chemical heterogeneity into account. Tenney et al.[5] carried out molecular simulations to

investigate the influence of surface heterogeneity upon predicted adsorption behavior in functionalized slit-pores. The following two types of heterogeneous structures were studied: the graphite edge sites with dangling bonds occupied by hydroxyl (−OH) or carboxyl (−COOH) groups and the graphene basal plane with defects and oxygen functional groups. The force field parameters for the various elements were either taken from the literature or calculated on the basis of results obtained from ab initio calculations for ∼100-atom polycyclic aromatic hydrocarbons at the HF/6-31g(d,p) level of theory along with a Mulliken charge analysis. However, according to the previous experimental and theoretical work carried out by Kudin et al.,[28] hydroxyl groups do not exist at edge sites but only as active sites on the basal surface. It is crucial to investigate functional groups that reflect realistic flue gas conditions in the case of carbon capture or geologic conditions in the case of storage. Furthermore, additional oxygen-containing functional groups, such as carbonyl and epoxy, which inherently exist in the structure of coal,[14,28] have not been included in previous molecular simulation studies concerning $CO_2$ adsorption.

The objectives of this work were to evaluate the influence of realistic surface functional groups of carbon pore surfaces on the adsorption of $CO_2$. Plane-wave electronic structure calculations were performed to determine the electrostatic distribution of the functionalized carbon surfaces. A Bader charge analysis[29] was undertaken to calculate the partial charge distributions, which were required for the energy contributions in the statistical model simulations. In particular, Monte Carlo (MC) simulations were carried out within the grand canonical ensemble to predict the thermodynamic equilibrium properties of the $CO_2$−carbon pore system.

## 2. COMPUTATIONAL METHODOLOGY

**2.1. Density Functional Theory (DFT).** Electronic structure calculations of functionalized carbon surfaces were carried out using the Vienna ab initio simulation package (VASP).[30,31] Plane-wave electronic density functional theory was employed due to its balanced computational efficiency and reasonable accuracy in predicting the partial charge distributions. The DFT calculations coupled with a van der Waals-inclusive correction (DFT-D)[32] were carried out to calculate the energies associated with the interlayer interactions of

graphitic structures, and the corresponding partial charge values associated with the top layer atoms were compared with the values given by DFT calculations without the corrections. The projector augmented wave (PAW) potential[33,34] was used to describe the core–valence electron interaction of the carbon and oxygen atoms. The model of Perdew, Burke, and Ernzerhof (PBE)[33] was employed for the non-local corrections, and an 11 × 11 × 1 Monkhorst–Pack[35] $k$-point sampling grid with a plane-wave cutoff of 750 eV was used. An idealized perfect and functionalized carbon-based pore surface was represented by a three-layer graphite slab. Previous investigations[26,36] have confirmed that three graphene layers are sufficient to model the $CO_2$–surface interactions within a slit pore comprised of a graphite framework due to the weak influence that the neighboring carbon layers have on the adsorption energy. Given the periodic boundary conditions, a vacuum region of 20 Å between the slabs was used to prevent interactions between the periodic images. The investigated systems include a perfect graphite basal plane surface, a hydrated graphite surface, and five oxygen-containing functionalized-graphite surfaces, each with unique vacancy sites or functional groups. Previous DFT and experimental studies have investigated similar functional groups and have shown them to be stable on graphene or graphite surfaces. In addition, these functional groups are likely to exist in coal and the organic material of gas shale due to the presence of water vapor and subsequent water–surface interactions.[14] As shown in Figure 1, graphite surface functional groups of the following types were considered: monovacancy[27] (i.e., V1) with dissociated $H_2O$,[37] epoxy functionalized,[28] hydroxyl functionalized,[28,38] carbonyl functionalized,[38] and combined hydroxyl–carbonyl functionalized.[38]

The investigated functional groups were positioned on either a 6 × 6 (e.g., hydrated graphite surface) or a 4 × 4 (e.g., other embedded oxygen-contained functionalized surfaces) carbon-ring unit cell with functional groups located in the center of the top graphene layer. To balance the computational time and accuracy of the calculations, all of the atoms in the top two layers were allowed full flexibility, while the positions of the carbon atoms in the bottom layer were fixed. To allow a fair comparison among various functionalities, the O:C ratio of all functionalized surfaces was kept as 1:24, with the exception of the basal plane and hydrated graphite surface.

To investigate the relative reactivity of water vapor and $CO_2$ on the monovacancy site[27] and then to determine what the ultimate stable graphite surface is, the dissociation of water vapor and $CO_2$ was investigated. The adsorption energy can be calculated from eq 1:

$$E_{ads} = E_{surf+CO_2/H_2O} - E_{surf} - E_{CO_2/H_2O} \qquad (1)$$

The adsorption energies were compared, with the lower energy representing the more stable surface.

Bader charge analysis[29] was undertaken to calculate the partial charge distributions of the perfect graphite and the functionalized graphite surfaces, which were required for the energy contributions in the statistical model simulations.

**2.2. Molecular Simulations.** Grand canonical Monte Carlo (GCMC) simulations[39] of $CO_2$ adsorption in idealized organic microporous carbons were carried out in the $\mu$VT ensemble.[40] In the current work, to focus on the effect of the surface functionalities, conditions of 298 K and 1 atm were investigated, which are relevant to carbon capture applications. The Peng–Robinson equation of state was used to relate the bulk experimental pressure with the chemical potential required

in the GCMC simulations. To speed up the convergence, energy-biased insertions of the sorbate molecules were employed and acceptance ratios for insertions and deletions were above 1% (slightly lower at the higher loadings) to ensure good equilibration in GCMC simulations. A total of approximately 100 million GCMC moves were attempted during each GCMC simulation. To reduce the computational time, a rigid graphite framework was assumed. The rigid framework assumption is based on the fact that the graphitic structures have been optimized in the plane-wave DFT calculations and that the geometries of the framework were not significantly influenced by $CO_2$ adsorption.

Physisorption processes of $CO_2$ in microporous carbons are predominantly associated with van der Waals forces (also known as dispersion–repulsion forces) and electrostatic forces (also known as Columbic interactions), which are sourced mainly from permanent dipole, quadrupole, and higher-induced-pole interactions. The van der Waals forces are present in all systems, but the electrostatic interactions are only present in systems that contain charge, such as charge due to surface functional groups or surface defects.[41]

In the current work, the $CO_2$ molecule was represented by the TraPPE model,[42] a three-site rigid model that accounts for the intrinsic quadrupole moment of $CO_2$ using a partial charge at each site. The partial charges on C and O atoms are $q_C$ = 0.70 $e$ and $q_O$ = −0.35 $e$ ($e$ = 1.6022 × 10$^{-19}$ C), respectively. The $CO_2$ molecule has a C=O bond length of 1.16 Å, with an O=C=O bond angle of 180°. The $CO_2$–$CO_2$ interactions were modeled as a combination of Lennard-Jones (LJ) and Columbic potentials, where the van der Waals interactions between two Lennard-Jones (LJ) sites were calculated using the LJ 12-6 potential and the electrostatic interactions were calculated on the basis of the Bader charge analysis. The potential energies associated with different LJ sites were calculated using standard Lorentz–Berthelot mixing rules.[43] As shown in Table 1, The LJ parameters for the other species

**Table 1. Potential Parameters for Force Field Calculations**

|  |  | $\varepsilon_{ff}/k_B$ [K] | $\sigma_{ff}$ [Å] |
|---|---|---|---|
| TraPPE | C($CO_2$) | 27 | 2.8 |
|  | O($CO_2$) | 79 | 3.05 |
| C(graphite) |  | 28 | 3.4 |
| O(surface functional groups) |  | 79 | 3.1 |
| H(surface functional groups) |  | 30 | 1.31 |

contained within the surface functional groups were taken from previous molecular simulation studies of Tenney et al.[5]

In this work, the effects of carbon surface functionality on the adsorption of $CO_2$ were investigated by simulating $CO_2$ adsorption in idealized carbon frameworks with various embedded functional groups and surface defects, which were represented by the DFT-optimized perfect and functionalized graphitic slit pores.

Due to the potential existence of undercoordinated carbon atoms in the pore structures, the graphitic surfaces become reactive toward existing volatile components in the adsorbed mixtures, such as water vapor. In the case that temperature and pressure conditions favor surface-bound water or various forms of dissociated water, the $CO_2$–surface adsorption may be passivated or enhanced due to the existence of oxygen-containing functional groups.
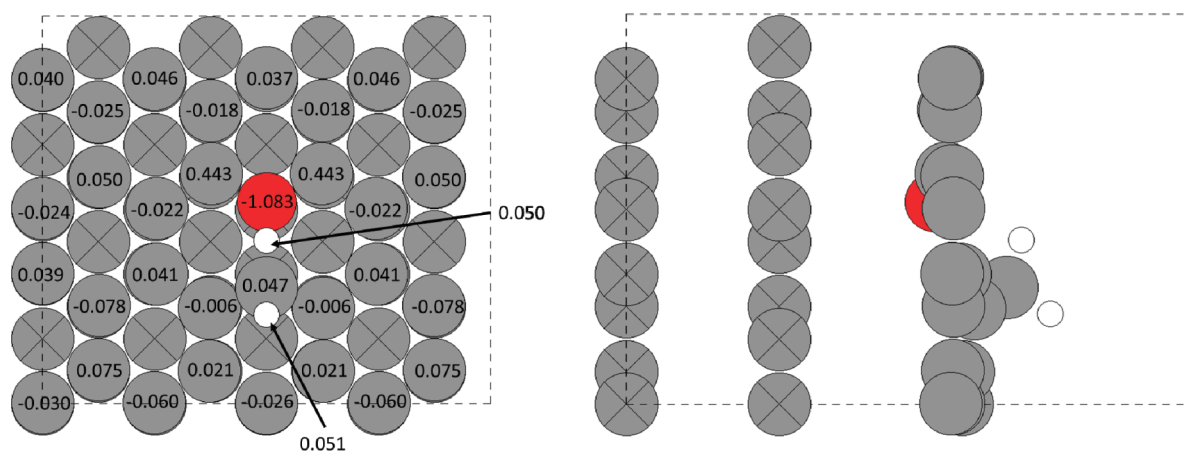
**Figure 2.** Partial charge distribution of hydrated graphitic surface (dissociated $H_2O$ on the monovacancy site of the top layer graphene surface): left, top view; right, side view; gray, carbon atoms (cross represents bottom two layers); red, oxygen atom; white, hydrogen atoms.

In addition, there may be inherent functional groups in the natural systems including oxygen, hydrogen, nitrogen, and sulfur atoms. As discussed in section 2.1, the functional groups investigated in the current work include epoxy, hydroxyl, and carbonyl chemistries.

For both lab measurements and molecular simulations, it is essential to accurately determine the pore volume available for adsorption. Given that helium is a nonadsorbing gas (or very weakly adsorbing gas), the pore volume is typically determined using helium at ambient temperature before initiating adsorption experiments. While the pore volume accessed by helium is not necessarily the same as that by $CO_2$ at the same temperature and pressure conditions, the helium pore volume measurements may accurately describe the trend associated with the pore volume as it is influenced by the various functional groups. Furthermore, the helium pore volume measurements were conducted using GCMC in this work for consistency with experimental work, in which helium pore volume measurements are widely used. The detailed algorithm associated with the pore volume calculation using helium is available in the Supporting Information.

## 3. RESULTS AND DISCUSSION

**3.1. Bader Charge Analysis of the Perfect and Functionalized Graphitic Surfaces.** In the current work, the two most stable configurations of dissociated $H_2O$ suggested by Kostov et al.[37] and one configuration of dissociated $CO_2$[44] on the monovacancy site of a three-layer graphite slab have been investigated. The equilibrium interlayer distance of perfect graphite was calculated by the DFT-D method as 3.47 Å, which compares well against the experimental measurement of 3.35 Å,[45] with an error of within 4%. The GGA functionals are unable to describe nonlocal dispersive interactions, and therefore, the interlayer distance cannot be optimized accurately by the DFT calculations without the van der Waals-inclusive correction. The two hydrated graphitic surfaces examined in the current work have DFT-D predicted zero-pressure and zero-temperature adsorption energies of ca. −102 and −91 kcal/mol. As a comparison, the predicted adsorption energies of the two hydrated graphene surfaces are ca. −102 and −92 kcal/mol, compared to the predicted literature values of −87 and −76 kcal/mol for similar graphene surfaces reported for dissociated $H_2O$ on the monovacancy site.[37] The reason for the lower predicted

adsorption energies of the previous work is due to the different reference point chosen by Kostov et al., who chose the relaxed physisorbed water molecule over the center of the vacancy as the energy reference. To investigate the effect of the van der Waals correction, the predicted adsorption energies of the two hydrated graphitic surfaces are ca. −97 and −87 kcal/mol without the van der Waals correction, respectively. We conclude that a single-layer graphene surface may be sufficient to determine the trend of the adsorption energies for different hydrated surfaces, but the effect of the nonlocal dispersive interactions cannot be neglected in predicting adsorption energies accurately when the graphite model is considered. Compared to dissociated $H_2O$ at the monovacancy defect site, $CO_2$ has a higher adsorption energy (ca. −42 kcal/mol) and thus is less stable. The optimized geometries of these three configurations are available in the Supporting Information. At a given pressure and temperature, the monovacancy defect site with dissociated $H_2O$ yields a lower surface free energy; therefore, dissociated $H_2O$ is more likely than $CO_2$ dissociation or chemisorption. Rather than $CO_2$ interacting directly with the monovacancy, $CO_2$ is more likely to react indirectly via a dissociated $H_2O$ molecule. This indicates that it is crucial to take surface chemical heterogeneity into account for determining $CO_2$ adsorption mechanisms in micropores for real systems.

Figure 2 shows the results of a Bader charge analysis of the most stable hydrated graphite surface carried out in the current work. For atoms that have a higher electron density compared to the original neutral atom, the negative partial charge values represent the gain in electrons from the other surface atoms. These electronegative atoms have an increased potential to donate electrons to the gas-phase molecules in the pore space, such as $CO_2$ in this case. Therefore, as Figure 2 indicates, the oxygen atom is highly electronegative and thus can serve as a basic adsorption site on the basal plane. The partial charge values calculated based on the DFT-D method were compared with the results given by the electronic structure calculations without the van der Waals correction. It was found that the maximum difference in the charge associated with the top-layer atoms is lower than 1%, which minimally impacts the GCMC simulations. Therefore, the corrections were neglected for the GCMC simulations. Due to the balanced computational efficiency and reasonable accuracy, the Bader charge results based on the DFT calculations were employed in the molecular simulations.
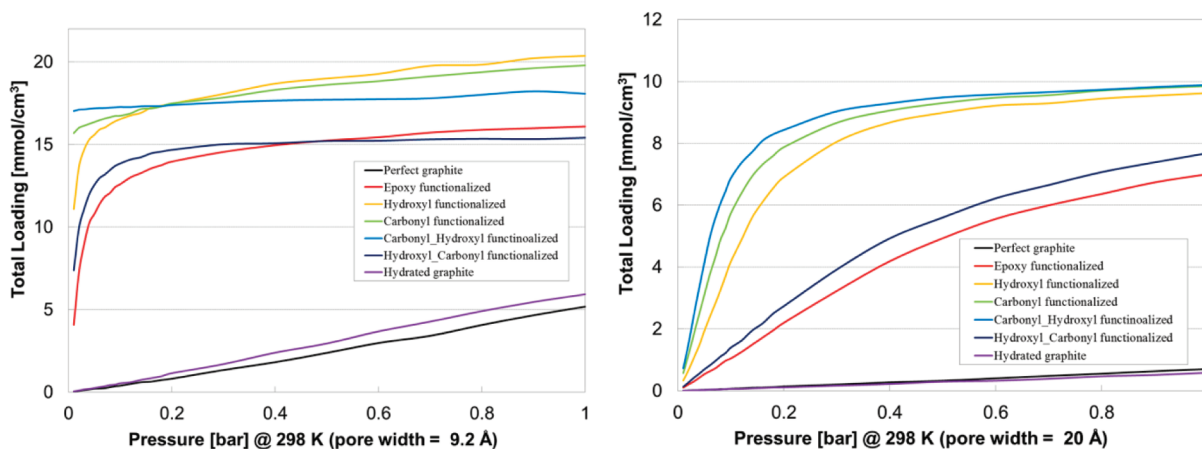
**Figure 3.** Comparison of $CO_2$ adsorption isotherms in slit pores with different embedded surface functional groups.
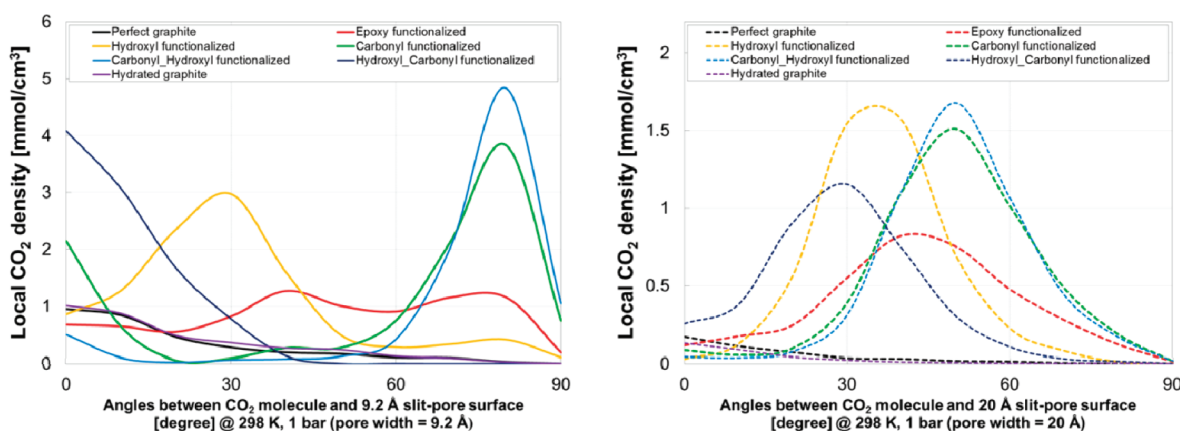


**Figure 4.** Orientation distribution of $CO_2$ in the functionalized micropores.

Except for the functional groups formed due to the competition of volatile components, such as $H_2O$, as discussed in the previous section, the partial charge distribution of the embedded oxygen-containing functional groups have also been considered. Similar to hydrated graphite surfaces with dissociated $H_2O$ on the monovacancy defect site, the embedded oxygen atoms on each surface show high electronegativities, because they gain electrons from the surrounding surface carbon atoms. For example, oxygen contained within a carbonyl functional group has a partial charge of $-1.047$ $e$ and therefore has the highest potential among all the surface atoms to donate electrons to the neighboring gas molecules. Due to the higher electronegativities of the O atoms than the C atom of $CO_2$ molecules, the C atom will be more attracted to the embedded oxygen functional groups. It is expected that the packing pattern of the adsorbed $CO_2$ molecule will be influenced upon the basis of this interaction and the $CO_2$ adsorption will be enhanced or passivated by the presence of embedded oxygen functional groups. The overall results of the Bader charge analyses for all functionalized surfaces investigated are available in the Supporting Information. On the basis of the Bader charge analyses, graphitic slit pores with embedded hydroxyl and carbonyl functional groups are hypothesized to more strongly influence surface−$CO_2$ interactions compared to the other functional groups investigated.

**3.2. Adsorption of $CO_2$ in Perfect and Functionalized Slit Pores.** The unit cell volumes of the micropores with the same pore width have been compared. All of the pore volumes

have been normalized to the perfect graphite slit pores with the corresponding pore width. For pores approximately 9.2 and 20 Å wide, it is important to note that the actual pore volume varies due to the different geometries of the functional groups present, even though the pore widths themselves are equal. For example, compared to the slit pore with a perfect graphite surface, an epoxy functional group embedded in the top layer of the graphite surface in a 9.2 Å pore decreases the volume by approximately 15%. A complete summary of the comparison of pore volumes with different surface functionalities is available in the Supporting Information.

Figure 3 shows the comparison of $CO_2$ adsorption isotherms for hydrated graphitic slit pores and different functionalized graphitic slit pores. The total loadings represent the total amount of $CO_2$ (including $CO_2$ in both condensed surface-bound and gas phases) per unit pore volume. In micropores where the diameter is less than 2 nm,[46] adsorption is governed by $CO_2$−surface interactions with wall−wall interactions also playing a significant role. In general, the oxygen-containing functional groups increase the adsorbed $CO_2$ density in the micropore structure, especially in the cases of hydroxyl- and carbonyl-functionalized graphitic slit pores. These results are consistent with the electronic structure predictions, in that the higher electron densities surrounding the oxygen atoms of functional groups attract more $CO_2$. On the other hand, the hydrated graphite was found to hinder $CO_2$ adsorption. It is important to note that due to the induced polarity of the surface functionalization, water vapor will always preferentially
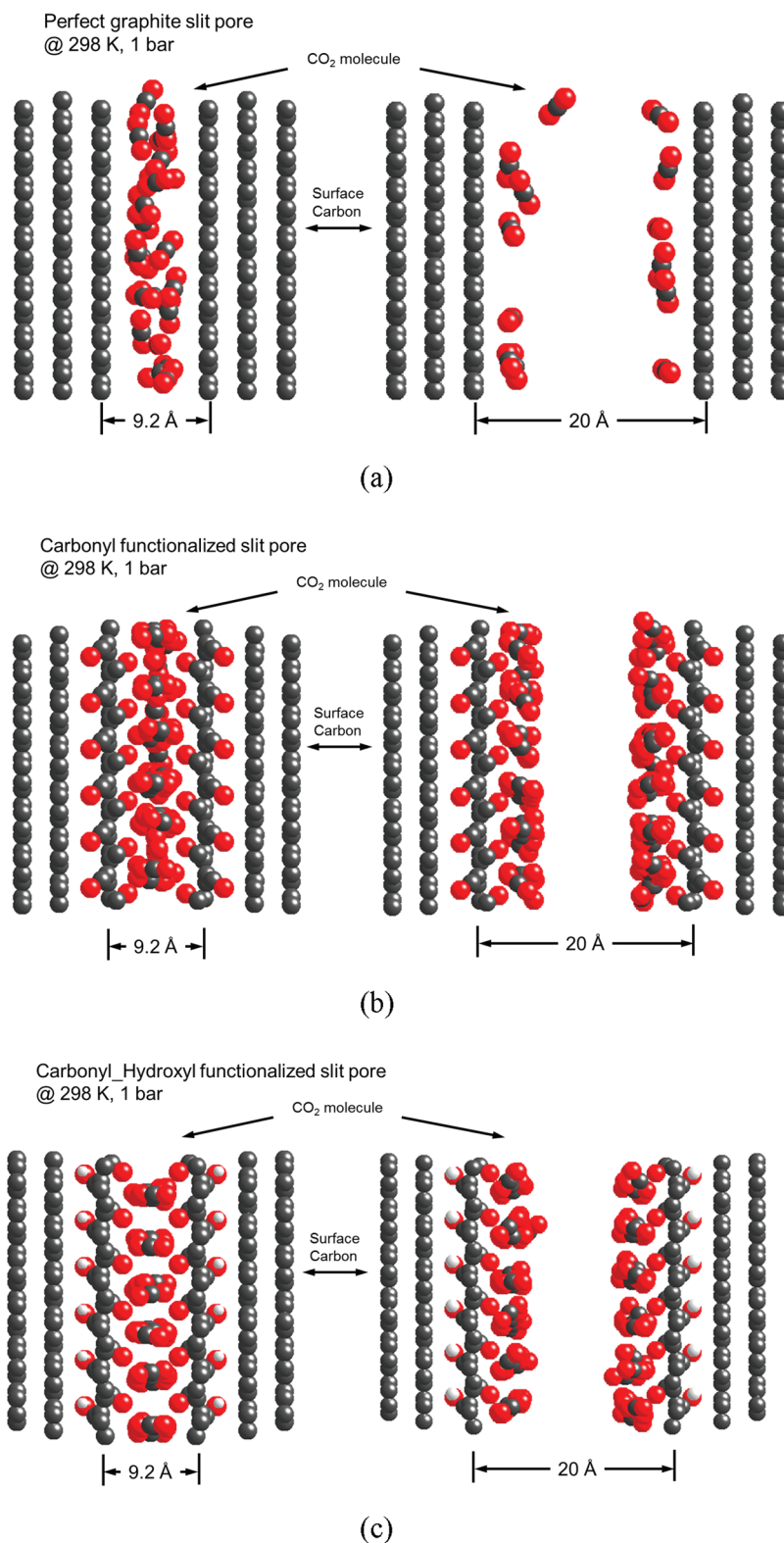
**Figure 5.** Comparisons of $CO_2$ adsorbed in functionalized micropores with that in the perfect graphite slit pore: left, side views of adsorbed $CO_2$ in various functionalized graphite slit pores with pore width of 9.2 Å; right, side views of adsorbed $CO_2$ in various functionalized graphite slit pores with pore width of 20 Å.

adsorb over $CO_2$ to these surfaces. This is due to the dipole moment of water having a stronger effect than the quadrupole moment of $CO_2$. As water vapor is present in flue gas at an approximate 10% concentration compared with $CO_2$ at ~12−14%, it is important to design sorbents that lead to water's

participation, as it will always be more "reactive" than $CO_2$, based upon charge.

A general noticeable shortcoming of adsorption-based $CO_2$ separation processes is that competing gases like $H_2O$ usually need to be removed upstream because of their high polarity,

and therefore, they might be preferentially adsorbed on the sorbent, thereby reducing its capacity for $CO_2$. Future work will involve the effect of $H_2O$ on the adsorption of $CO_2$, as well as mixtures including $CO_2/CH_4$, $CO_2/N_2$, etc.

To further explore the packing patterns of adsorbed $CO_2$ molecules, the local adsorbed $CO_2$ densities at different $CO_2$ orientations were compared among different investigated embedded functional groups, as shown in Figure 4. In the perfect graphite slit pore the $CO_2$ molecules are aligned mostly parallel to the pore surfaces. In the 9.2 Å pore, due to the overlapping potentials from the strong pore wall–wall interations, the carbonyl functional group on the surface influences the $CO_2$ orientation profile significantly, with the majority of the $CO_2$ molecules oriented perpendicular to the surface. However, in the case of the hydroxyl functional group embedded surface, the $CO_2$ molecules are oriented at approximately 30° or less with respect to the pore wall. Similarly, in the 20 Å pores, due to the weaker surface–surface interactions, the majority of the $CO_2$ molecules are rotated approximately 60° with respect to the surface with carbonyl functional groups and are orientated at approximately 30° to the surface with hydroxyl functional groups upon adsorption. The functionality-induced packing pattern makes it more efficient for $CO_2$ to occupy the limited pore space, with this change in packing pattern allowing for enhanced $CO_2$ adsorption capacity in the slit pores with hydroxyl and carbonyl functional groups than without.

To have an improved understanding of the $CO_2$ packing, snapshots of $CO_2$ in the functionalized graphitic surfaces at 1 bar are shown in Figure 5. From Figure 5, the following can be observed: (1) the $CO_2$ molecules are more organized and aligned when they are adsorbed in the functionalized slit pores, and thus the adsorption capacity is enhanced by the higher efficient side-by-side packing; (2) in the ultramicropores (ultramicropores have an average pore diameter of less than 7 Å as defined by IUPAC[46]), due to the overlapping potentials from the strong pore wall–wall interactions and the strong $CO_2$–wall interaction, the condensed adsorbed-$CO_2$ density is even higher than that of the larger pores. In general, as the pore width decreases, the surface functionalities dictate the adsorption, and thus the surface functionalities play a more important role in increasing the $CO_2$ adsorption capacity. The surface heterogeneity changes the adsorbates' accumulation configuration by changing the geometry of the pore surface and the charge distribution of the surface, which is consistent with the Bader charge results of DFT study.

The diffusion of $CO_2$ into ultramicropores is of particular concern for microporous carbons, especially for the scale of $CO_2$ emissions considered from large-scale point sources. The critical temperature of $CO_2$ is ~304 K and the corresponding saturation pressure is ~74 bar. In the case of $CO_2$ capture, the pressure that is relevant to $CO_2$ capture is in the range of moderate conditions.[47] Therefore, due to the low relative pressure and high relative temperature, $CO_2$ has the potential to enter the ultramicropores. It also should be noted that functionalized carbons, such as carbon molecular sieves and activated carbon, have inherently high surface areas due to the fact that they are primarily comprised of micropores and in some cases mesopores (typically less than 3−5 nm). It is unlikely that the active sites of these materials exist at the pore entrances; however, examining the barriers associated with entrance and exits of pores will aid in modifying these materials

for enhancing their kinetic performance, which will be investigated in our future work

On the basis of the assumption that the carbon-based sorbent density is between 500 and 1000 kg/m$^3$ and the porosity is around 0.5,[41] the total $CO_2$ loading is up to ~10 mmol/g in the microporous carbons at 1 bar according to the current GCMC simulation, compared to current state-of-the-art MOFs that range between 2 and 12 mmol/g at similar temperature and pressure conditions, based on experimental and theoretical studies.[48] Therefore, carbon-based sorbents may be competitive with other sorbents in terms of the capacity, e.g., zeolites and MOFs. It is important to note that the surface functionality of GCMC simulations is easily modified, allowing for a large number of sorbent materials to be screened to provide focus and insight into promising sorbents for further synthesis and experimental testing. Future work will involve molecular dynamics simulations and breakthrough experiments to test adsorption kinetics of functionalized graphitic micropores, as well as adsorption experiments to measure adsorption isotherms. The adsorption equilibrium measurements will be compared to the GCMC simulation results to determine the sorbent capacity and adsorption mechanisms more accurately.

## ■ ASSOCIATED CONTENT

### Ⓢ Supporting Information

Figure S1 provides the optimized geometries of $H_2O$ and $CO_2$ dissociation on the monovacancy site of the top layer of a graphite slab; details of the prediction of pore volume by helium adsorption from calculation of the second virial coefficient and the comparison of the realistic pore volumes with different surface functionalities are available; Figure S4 shows the partial charge distributions of various oxygen-containing functionalized graphite surfaces, and Figure S5 is a complete summary of the snapshots of $CO_2$ adsorbed in functionalized micropores. This material is available free of charge via the Internet at http://pubs.acs.org.

## ■ AUTHOR INFORMATION

### Corresponding Author

*Phone: 650 724 9449; fax: 650 725 2099; e-mail: wilcoxj@stanford.edu.

## ■ ACKNOWLEDGMENTS

## ■ REFERENCES

(1) U.S. Department of Energy. *Basic Reseach Needs for Carbon Capture: Beyond 2020*; DOE: Washington, DC, 2010. Available at http://www.sc.doe.gov/bes/reports/files/CCB2020_rpt.pdf

(2) Benson, S.; Cook, P. *Intergovernmental Panel on Climate Change, Special Report on Carbon dioxide Capture and Storage: Underground Geological Storage*; Cambridge University Press: Cambridge, UK, 2005; Chapter 5, pp 196−276.

(3) Bhatia, S. K.; Tran, K.; Nguyen, T. X.; Nicholson, D. High-pressure adsorption capacity and structure of $CO_2$ in carbon slit pores: Theory and simulation. *Langmuir* **2004**, *20*, 9612−9620.

(4) Kurniawan, Y.; Bhatia, S. K.; Rudolph, V. Simulation of binary mixture adsorption of methane and $CO_2$ at supercritical conditions in carbons. *AIChE J.* **2006**, *52* (3), 957−967.

(5) Tenney, C. M.; Lastoskie, C. M. Molecular simulation of carbon dioxide adsorption in chemically and structurally heterogeneous porous carbons. *Environ. Prog.* **2006**, *25* (4), 343−354.

(6) Kowalczyk, P.; Furmaniak, S.; Gauden, P. A.; Terzyk, A. P. Carbon dioxide adsorption-induced deformation of microporous carbons. *J. Phys. Chem. C* **2010**, *114*, 5126−5133.

(7) Lastoskie, C.; Gubbins, K. E.; Quirket, N. Pore size heterogeneity and the carbon slit pore: A density functional theory model. *Langmuir* **1993**, *9*, 2693−2702.

(8) Hu, X.; Radosz, M.; et al. $CO_2$-filling capacity and selectivity of carbon nanopores: Synthesis, texture, and pore-size distribution from quenched-solid density functional theory (QSDFT). *Environ. Sci. Technol.* **2011**, *45* (16), 7068−7074.

(9) Müller, E. A. Adsorption of super greenhouse gases on microporous carbons. *Environ. Sci. Technol.* **2005**, *39* (22), 8736−8741.

(10) Zhu, D.; Kwon, S.; Pignatello, J. J. Adsorption of single-ring organic compounds to wood charcoals prepared under different thermochemical conditions. *Environ. Sci. Technol.* **2005**, *39* (11), 3990−3998.

(11) Jorge, M.; Schumacher, C.; Seaton, N. A. Simulation study of the effect of the chemical heterogeneity of activated carbon on water adsorption. *Langmuir* **2002**, *18* (24), 9296−9306.

(12) White, C. M.; Smith, D. H.; Jones, K. L.; Goodman, A. L.; Jikich, S. A.; LaCount, R. B.; et al. Sequestration of carbon dioxide in coal with enhanced coalbed methane recovery—A review. *Energy Fuels* **2005**, *19*, 659−724.

(13) Haenel, M. W. Recent progress in coal structure research. *FUEL* **1992**, *71*, 1211−1223.

(14) Van Krevelen, D. W. *Coal*, 3rd ed.; Elsevier: Amsterdam, The Netherland, 1991.

(15) Zhao, J. J.; Buldum, A.; Han, J.; Lu, J. P. Gas molecule adsorption in carbon nanotubes and nanotube bundles. *Nanotechnology* **2002**, *13* (2), 195−200.

(16) Yim, W. L.; Byl, O.; Yates, J. T.; Johnson, J. K. Vibrational behavior of adsorbed $CO_2$ on single-walled carbon nanotubes. *J. Chem. Phys.* **2004**, *120* (11), 5377−86.

(17) Matranga, C.; Chen, L.; Smith, M.; Bittner, E.; Johnson, J. K.; Bockrath, B. Trapped $CO_2$ in carbon nanotube bundles. *J. Phys. Chem. B* **2003**, *107*, 12930−12941.

(18) Matranga, C.; Chen, L.; Bockrath., B.; Johnson, J. K. Displacement of $CO_2$ by Xe in single-walled carbon nanotube bundles. *Phys. Rev. B* **2004**, *70* (165416), 1−7.

(19) Cinke, M.; Li, J.; Bauschlicher, C. W.; Ricca, A.; Meyyappan, M. $CO_2$ adsorption in single-walled carbon nanotubes. *Chem. Phys. Lett.* **2003**, *376*, 761−766.

(20) Jiang, J. W.; Sandler, S. I. Separation of $CO_2$ and $N_2$ by adsorption in C168 Schwarzite: A combination of quantum mechanics and molecular simulation study. *J. Am. Chem. Soc.* **2005**, *127*, 11989−11997.

(21) Chen, L.; Johnson, J. K. Formation of odd-numbered clusters of $CO_2$ adsorbed on nanotube bundles. *Phys. Rev. Lett.* **2005**, *94* (12), 125701.

(22) Xu, S. C.; Irle, S.; Musaev, D. G.; Lin, M. C. Quantum chemical prediction of reaction pathways and rate constants for dissociative adsorption of $CO_x$ and $NO_x$ on the graphite (0001) surface. *J. Phys. Chem. B* **2006**, *110* (42), 21135−21144.

(23) Rivera, J. L.; McCabe, C.; Cummings, P. T. Layering behavior and axial phase equilibria of pure water and water + carbon dioxide inside single carbon nanotubes. *Nano Lett.* **2002**, *2*, 1427−1431.

(24) Allouche, A.; Ferro, Y. Dissociative adsorption of small molecules at vacancies on the graphite (0001) surface. *Carbon* **2006**, *44*, 3320−3327.

(25) Montoya, A.; Mondragon, F.; Truong, T. N. $CO_2$ adsorption on carbonaceous surface: A combined experimental and theoretical study. *Carbon* **2003**, *41*, 29−39.

(26) Cabrera-Sanfelix, P. Adsorption and reactivity of $CO_2$ on defective graphene sheets. *J. Phys. Chem. A* **2009**, *113* (2), 493−498.

(27) Hashimoto, A.; Suenaga, K.; Gloter, A.; Urita, K. Direct evidence for atomic defects in graphene layers. *Nature* **2004**, *430* (19), 870−873.

(28) Kudin, K. N.; Ozbas, B.; Schniepp, H. C.; Prud'homme, R. K.; Aksay, I. A.; Car, R. Raman spectra of graphite oxide and functionalized graphene sheets. *Nano Lett.* **2008**, *8* (1), 36−41.

(29) Bader, R. F. W. *Atoms in Molecules: A Quantum Theory*. Oxford University Press: New York, 1990.

(30) Kresse, G.; Furthmüller, J. Efficiency of ab initio total energy calculations for metals and semiconductors using a plane-wave basis set. *Comput. Mater. Sci.* **1996**, *6*, 15−50.

(31) Kresse, G.; Hafner, J. Ab initio molecular dynamics for open-shell transition metals. *Phys. Rev. B* **1993**, *48*, 13115−13118.

(32) Grimme, S. Semiempirical GGA-type density functional constructed with a long-range dispersion correction. *J. Comput. Chem.* **2006**, *27*, 1787−1799.

(33) Perdew, J. P.; Burke, K.; Ernzerhof, M. Generalized gradient approximation made simple. *Phys. Rev. Lett.* **1996**, *77*.

(34) Kresse, G.; Joubert, D. From ultrasoft pseudopotentials to the projector augmented-wave method. *Phys. Rev. B* **1999**, *59*, 1758−1775.

(35) Monkhorst, H. J.; Pack, J. D. Special points for Brillouin-zone integrations. *Phys. Rev. B* **1976**, *13*, 5188−5192.

(36) Sanfelix, P. C.; Holloway, S.; Kolasinski, K. W.; Darling, G. R. The structure of water on the (0001) surface of graphite. *Surf. Sci.* **2003**, *532−535*, 166−172.

(37) Kostov, M. K.; Santiso, E. E.; Gubbins, K. E.; Nardelli, M. B. Dissociation of water on defective carbon substrates. *Phys. Rev. Lett.* **2005**, *95*, 136105.

(38) Bagri, A.; Grantab, R.; Medhekar, N. V.; Shenoy, V. B. Stability and formation mechanisms of carbonyl- and hydroxyl-decorated holes in graphene oxide. *J. Phys. Chem. C* **2010**, *114*, 12053−12061.

(39) Frenkel, D.; Smit, B. *Understanding Molecular Simulation*, 2nd ed.; Academic Press: New York, 2001.

(40) Gupta, A.; Chempath, S.; Sanborn, M. J.; Clark, L. A.; Snurr, R. Q. Object-oriented programming paradigms for molecular modeling. *Mol. Simul.* **2003**, *1* (29), 29−46.

(41) Wilcox, J. *Carbon Capture*; Springer Publishing: New York, 2012.

(42) Potoff, J.; Siepmann, J. Vapor−liquid equilibria of mixtures containing alkanes, carbon dioxide and nitrogen. *AIChE J.* **2001**, *47*, 1676−1682.

(43) Allen, M. P.; Tildesley, D. J. *Computer simulation of liquids*; Clarendon Press, 1989.

(44) Liu, Y.; Wilcox, J. $CO_2$ adsorption on carbon models of organic constituents of gas shale and coal. *Environ. Sci. Technol.* **2011**, *45* (2), 809−814.

(45) Zhao, Y. X.; Spain, I. L. X-ray diffraction data for graphite to 20 GPa. *Phys. Rev. B: Condens. Matter* **1989**, *40*, 993−997.

(46) Sing, K. S. W.; Everett, D. H., et al. *Reporting Physisorption Data for Gas/Solid Systems. Handbook of Heterogeneous Catalysis*. Wiley-VCH: Weinheim, Germany, 2008.

(47) Lowell, S.; Shields, J. E.; Thomas, M. A., et al. *Characterization of Porous Solids and Powders: Surface Area, Pore Size and Density*; Springer: New York, 2006.

(48) D' Alessandro, D.; Smit, B.; Long, J. R. Carbon dioxide capture: Prospects for new materials. *Angew. Chem., Int. Ed.* **2010**, *49*, 6058−6082.